Abnormal patterns of sleep and waking behaviors are accompanied by increased slow gamma power in an Ank3 mouse model of epilepsy-bipolar disorder comorbidity

Angel Lopez (alopez0843@utexas.edu)
University of Texas at Austin
Juan Villacres
University of Texas at Austin
Nicholas Riveira
University of Texas at Austin
Sohmee Kim
University of Texas at Austin
Laura Colgin
University of Texas at Austin
Jeffery Noebels
Department of Neurology, Baylor College of Medicine

Article

Keywords: ANK3, Ankyrin-G, bipolar disorder, epilepsy, slow gamma rhythms, sleep

Posted Date: May 9th, 2022

DOI: https://doi.org/10.21203/rs.3.rs-1617910/v1

Additional Declarations: The authors have declared there is **NO** conflict of interest to disclose

Version of Record: A version of this preprint was published at Translational Psychiatry on December 20th, 2023. See the published version at https://doi.org/10.1038/s41398-023-02700-2.

Abstract

ANK3 is a leading bipolar disorder candidate gene in humans. Previous studies showed that deletion of *Ank3-1b,* a bipolar disorder (BD)-associated variant of *Ank3* in mice leads to increased firing threshold and diminished action potential dynamic range of parvalbumin (PV)-interneurons and absence epilepsy, thus providing a biological mechanism linking epilepsy and BD. To better understand the impact of defective PV interneurons on network activity and behavior in these mice, we examined spectral EEG correlates of behaviors seen in *Ank3-1b* knockout (KO) mice during home-cage activity using paired video-EEG recordings. Since PV-interneurons contribute to the generation of high frequency gamma oscillations, we anticipated changes in the power of EEG signals in the gamma frequency range (> 25 Hz) during behavioral deficits related to human BD symptoms, including abnormal sleep and activity levels. *Ank3-1b* KO mice exhibited an overall increase in slow gamma (~25-45 Hz) power compared to controls, and slow gamma power correlated with seizure phenotype severity across behaviors. During sleep, increased slow gamma power correlated with decreases in time spent in the rapid eye movement (REM) stage of sleep. Seizures were more common during REM sleep compared to non-REM (NREM) sleep. We also found that *Ank3-1b* KO mice were hyperactive and exhibited a repetitive behavior phenotype that correlated with increased slow gamma power. Our results identify a novel EEG biomarker associating *Ank3* genetic variation with BD and suggest modulation of gamma oscillations as a potential therapeutic target.

INTRODUCTION

Bipolar disorder (BD) is a highly heritable, genetically complex, and debilitating mood disorder with a high incidence of suicide[1]. While little is known about the neurophysiology underlying BD, significant advances have been made in the identification of BD-associated genes. ANK3 has been identified as a leading BD candidate gene through various human genetics studies. Rare variants of significant effect in coding regions of ANK3 have been identified in families with BD and mood-related psychiatric symptoms[2–4], and common variants in noncoding regions of ANK3 have more widely shown associations with BD through multiple, independent genome-wide association studies (GWAS)[5–10]. These GWAS show a hotspot for single nucleotide polymorphisms (SNPs) in an intronic, candidate cis-regulatory region upstream of ANK3's third alternative-first-exon (exon-1b). Human studies suggest that these SNPs are associated with reduced expression of ANK3 transcripts and are accompanied by altered neuropathology[11–13].

ANK3 is a very large gene that undergoes significant alternative splicing to produce various isoforms of the scaffolding protein, Ankyrin-G (AnkG). ANK3 has three alternative-first-exons, two of which are utilized by neurons and glia in the brain (exon-1e and exon-1b) to transcribe three main groups of AnkG isoforms with different functions. The 480 kDa group of isoforms are found at GABAergic synapses and the axon initial segment (AIS) of neurons[14]. At the AIS, exon-1e and exon-1b code for alternative N-termini (NT2 and NT3, respectively) of AnkG which serve to regulate the binding of sodium and potassium channels to the adjacent membrane binding domain[15].

Our previous study discovered that GABAergic parvalbumin (PV)-interneurons exclusively express NT3-AnkG isoforms at the AIS, while excitatory pyramidal cells in many brain regions express NT2-AnkG. This work showed that PV-interneurons in *Ank3-exon1b* (*Ank3-1b*) knockout (KO) mice have a reduced number of voltage-gated sodium channels at the AIS, increased firing threshold, and diminished action potential dynamic firing range at frequencies above 100 Hz[16]. Additionally, this work showed that *Ank3-1b* deletion results in reduced cortical network inhibition and an absence epilepsy phenotype that was recapitulated by knocking out all AnkG isoforms selectively in PV-interneurons. This makes *Ank3-1b* mice a unique model for studying epilepsy-bipolar disorder comorbidity which studies show is significant and bidirectional but has not been well explored[17–19]. These findings led to the hypothesis that imbalanced excitation and inhibition due to PV interneuron dysfunction may underlie the genetic association between ANK3 and BD and serve as a shared mechanistic link connecting thalamocortical epilepsy and mood disorder.

PV interneuron deficiencies and aberrant gamma rhythms have been implicated in BD through human studies[20–24], and a familial mutation of ANK3 (W1989R) caused disrupted cortical and hippocampal gamma oscillations in a knock-in mouse model[3]. The fast-spiking properties of PV interneurons are important for generating and modulating high frequency gamma oscillations[25]. Thus, we hypothesized changes in the power of gamma oscillations in *Ank3-1b* KO mice. Additionally, we hypothesized that changes in gamma power would be accompanied by changes in behaviors relevant to BD in this model. Previous behavioral studies of *Ank3-1b* heterozygous (*Ank3-1b*$^{+/KO}$) KO mice have been used to model BD. In this study, a battery of behavioral assays was used to phenotype *Ank3-1b*$^{+/KO}$ mice and found decreased anxiety, increased motivation for reward at baseline, and a transition to depression-related features after chronic stress via isolation[26]. However, the effect sizes were relatively small, making reproducibility a challenge for in vivo electrophysiological studies often limited in cohort size due to technical and time constraints. Also, brief behavioral assays may not capture mood oscillations congruent with those of BD patients which require study over longer periods of time.

One way to address these issues is to utilize recent high-throughput methods of monitoring rodent behavior over prolonged uninterrupted periods of home cage activity, allowing the study of some common endophenotypes of BD that have not yet been explored in this model, such as sleep disturbances and repetitive behaviors. In the present study, we employed an automated approach to behaviorally phenotype *Ank3-1b* mice using the open-source learning algorithm, DeepLabCut, while simultaneously examining gamma oscillations using paired video-EEG recordings taken from the *Ank3-1b* KO mice and their littermate controls[16].

MATERIALS AND METHODS

Animals

All studies here are secondary analyses of existing paired video-EEG recordings previously published[16]. This dataset utilized adult (6–8 weeks old) C57BL/6J *Ank3-1b*[27] mice bred from heterozygous crosses to generate test mice and littermate controls. Both sexes were included in our analyses. This dataset consisted of 4 wildtype (WT), 7 heterozygous *Ank3-1b*, and 7 homozygous *Ank3-1b* KO mice. However, only 3 WT, 4 heterozygous, and 6 homozygous mice had accompanying video data. Therefore, data from this subset were used for the behavior-related analyses, while all 18 mice were examined in the general EEG spectral analysis indiscriminate of behavioral state. One *Ank3-1b*$^{KO/KO}$ mouse was excluded from spectral analysis due to excessive seizure activity (average of ~ 665 seizures/hour representing 43.7% of the recording time). All mice were housed on a reverse light-dark cycle, and the animal procedures followed protocols approved by the IACUC committees of Baylor College of Medicine.

Video-electroencephalography

Video-EEG recording methods are described in detail previously[16]. Mice were surgically implanted with bilateral silver wire electrodes (0.005" diameter) inserted through cranial burr holes into the subdural space over the frontal and parietal cortices bilaterally. The electrodes were attached to a micro-miniature connector cemented to the skull, and simultaneous video-EEG recordings (Harmonie software version 6.1c, Stellate Systems) were obtained from freely moving mice in a home cage setup. The home cage setup consisted of a glass tank (LWH: 12.25" x 6.25" x 8.25") with an open lid, filled with ~ 1 inch of corn cob bedding and freely accessible food pellets and water. The cages were housed in facilities with restricted human access to minimize stress and interference. Behavior was monitored by video recording from a single camera angle, either perpendicular to the long side or short end of the cage.

Movement tracking and behavioral classification

We used DeepLabCut (DLC), an open-source marker-less pose estimation software[28], to track the position of freely moving mice in video recordings. Since video angles were not consistent across all mice and some videos contained multiple cages of singly housed mice, multiple models were trained to ensure high accuracy position tracking for all mice. In total, 7 different models were trained on various cage positions and video cropping parameters. From each set of videos with similar angles, 200–250 randomly selected frames were labeled, and its model trained through DeepLabCut using resources from the Texas Advanced Computing Center for 300,000 + iterations.

The position estimates gathered from DLC were used to build two types of classifiers. One type of classifier utilized linear discriminant analysis (LDA) models to classify awake behaviors. The other was a binary classifier based on previously published work[29] and was used to identify sleep episodes. Two hours of manually scored behaviors (i.e. walking, grooming, digging, awake rest, and sleep) from two mice per genotype were used as ground truth for training and validating each model.

For the sleep classifier, DLC data tracking each mouse's nose, front paws, hind paws, base of tail, and mid-body were used to evaluate the position centroids of each frame. Frame-by-frame centroid displacements were then evaluated to track each mouse's motion over time. Displacement percentiles

were then calculated for motion thresholding. The classifier's receiver operating characteristic (ROC) curve was generated using the manually scored data as ground truth to select the displacement threshold that provided optimal true positive and false positive rates, which was found to be the 85th percentile. A bout duration threshold of 40 seconds was also used as previously described[29]. All bouts in which the centroid displacement was lower than the 85th displacement percentile for at least 40 seconds were thus classified as sleeping bouts (Supplementary Fig. 1A).

Awake behaviors were classified using separate linear discriminant analysis (LDA) models. 140 features for building the LDA classifiers were generated from the DLC position data. The features consisted of the Euclidean distance, angles, and displacement vectors between each point. Manually scored data from each behavior was established as ground truth for training and cross validation. LDA models were built using MATLAB's fitcdiscr function. K-Fold cross-validation with 500 partitions followed by generation ROC curves was performed for each classifier to evaluate their performance (Supplementary Fig. 1B-E). The classifiers were subsequently used to identify grooming, digging, walking, and resting awake behaviors.

Signal processing and spectral analysis

We used a supervised learning algorithm, 'detect_SWDs'[30], to identify seizure events from EEG recordings for removal prior to spectral analyses. Seizure activity was defined by at least 3 consecutive spike and wave discharges (SWDs) with amplitudes greater than or equal to 2.5 × baseline voltages at frequencies of 5–10 Hz. A 'detect_SWDs' classifier was trained on one-hour EEG recordings from two homozygous *Ank3-1b* KO mice, and subsequently used to identify seizures in all mice. The accuracy of the trained classifier was 91.3%. SWD calls for all mice were visually verified using a 'detect_SWDs' GUI and cross-validated with previously hand-scored data to eliminate all false negative and false positive calls from the data. This algorithm allowed for indexing of validated SWDs from the raw EEG before spectral analyses.

Signals from the left frontal lobe, where the electrode furthest from the digitally averaged reference electrode was located, were used in all spectral analyses. Signals were first normalized to a variance of 1 and a mean of 0 using code from the spike wave detection toolbox[30] and low pass filtered at 50 Hz. Normalized power of the EEG signal was then estimated from signal frequencies 1–50 Hz in 0.2 Hz wide frequency bands. A Morlet wavelet transform of the EEG signal was used for estimating oscillatory power across frequencies as previously described[31,32], with a width parameter (σ) of 5 and a frequency resolution of 1 Hz. Average power spectra are presented with corresponding 95% bootstrapped confidence intervals that were created by randomly sampling power spectra from recordings during individual bouts of behavior.

For non-behavior-specific analyses of full EEG recordings, all interictal clips longer than 4 seconds were analyzed using the Morlet wavelet transform method described above. To obtain a single estimate of average slow gamma rhythm power, the mean power estimates across 25–45 Hz frequency bins were summed (Fig. 2B and 2C).

Statistics

All statistics were performed in SPSS (IBM, version 27.0). Data were analyzed using the generalized linear mixed model (GLMM) function. Genotype was included in each model as a fixed effect. Individual mice were subjects, with repeated measurements collected from each mouse. For sleep patterns analyses (Fig. 2A & D, Supplementary Fig. 2), repeated measures included hour (i.e., time of day when recording was collected) and sleep stage (i.e., REM vs NREM). A genotype by sleep stage interaction effect was also included in the model. For analysis of oscillatory power during sleep (Fig. 2B-C & E-F), repeated measures included hour, sleep stage, and rhythm type (i.e., delta, theta, and slow gamma). Genotype by sleep stage, genotype by rhythm type, and 3-way genotype by sleep stage by rhythm type interaction effects were also included in the model to test whether genotype differentially affected rhythms of different types and whether effects differed across sleep stages. For analysis of genotype differences on awake behaviors (Figs. 3A, D; 4A, D), repeated measures included hour and type of behavior. A genotype by behavior type interaction effect was also included in the model. When significant interaction effects were observed, analyses were performed separately for different behavior types, with hour as a repeated measure and genotype tested as a main effect. For analyses of oscillatory power during awake behaviors (Fig. 3C, F; 4C, F), repeated measures included hour and rhythm type. Also, a genotype by rhythm type interaction effect was included. When significant interaction effects were found, analyses were performed separately for different rhythms, with hour as a repeated measure and genotype tested as a main effect. Specific details for each comparison are provided in the results. When main effects of genotype were observed, all possible pairwise comparisons of genotypes were performed and adjusted for multiple comparisons using the sequential Bonferroni procedure.

RESULTS

Ank3-1b **dose-dependent increases in slow gamma oscillations correlate with epilepsy phenotype severity**

Previous characterization of *Ank3-1b* KO mice showed that both homozygous (*Ank3-1b*$^{KO/KO}$) and heterozygous (*Ank3-1b*$^{KO/+}$) KOs have frequent seizure episodes, with SWDs occupying approximately 4% of total EEG activity from *Ank3-1b*$^{KO/KO}$ mice[16]. Since SWD spiking occurs at 6–8 Hz, creating pronounced peaks in power spectra, and because these seizures are accompanied by behavioral arrest, it was important to remove these events from our analyses. To do this, we utilized a supervised learning algorithm to automatically identify seizures in the EEG data[30]. This algorithm identifies SWDs based on the weighed scores of three properties, 1.) ~ 6 Hz spiking frequency, 2.) ~ 16–32 Hz harmonic, and 3.) sharpness of spikes utilizing the DB4 wavelet. We trained this algorithm on EEG from the *Ank3-1b* model to identify SWDs (Fig. 1A & 1B) according to scores most resembling a subset of hand scored data and then visually verified the automated calls (Fig. 1C). This data was then used to index EEGs and remove SWDs before spectral analysis.

Spectral analysis of all EEG recordings, indiscriminate of behavior, was first conducted to look for potential large effects between genotypes (Fig. 1D). Statistically significant increases in slow gamma

power were seen in *Ank3-1b*$^{KO/KO}$ mice compared to WT and *Ank3-1b*$^{KO/+}$ animals (main effect of genotype: F = 7.422, df = 2, p = 0.006; *Ank3-1b*$^{KO/KO}$ vs WT: std error: ±1.50 a.u., p = 0.024; *Ank3-1b*$^{KO/KO}$ vs *Ank3-1b*$^{KO/+}$: std error: ±1.16 a.u., p = 0.015; Fig. 1E). This suggests a gene dose dependent effect of slow gamma, similar to that previously described with regard to seizure frequency[16]. Thus, we ran linear regression analysis to test the relationship between slow gamma power and seizure classification scores and found a statistically significant positive correlation (R^2 = 0.30, p = 0.02; Fig. 1F). These data indicate a relationship between seizure activity and slow gamma power in an *Ank3-1b* dosage-dependent manner.

Ank3-1b **KO mice exhibit sleep disturbances co-occurring with increased slow gamma power**

Sleep disturbance is symptomatic of BD and because sleep disturbances are present throughout all mood states of BD, we used an existing classifier[29] to analyze sleep patterns in *Ank3-1b* KO mice. We further used an algorithm that distinguishes REM and NREM in sleep EEG using the theta (6–10 Hz) to delta (2–5 Hz) power ratio[33,34]. Significant differences in overall sleep duration (i.e., number of minutes of sleep per hour) were not observed between genotypes (Supplementary Fig. 2A, generalized linear mixed model, main effect of genotype: F(2,81) = 1.4, p = 0.3). The number of sleep bouts per hour also were not significantly different across genotypes (Supplementary Fig. 2B, generalized linear mixed model, main effect of genotype: F(2,81) = 0.5, p = 0.6). However, we found that the effects of *Ank3-1b* deletion on sleep patterns differed across sleep stages, with sleep patterns more strongly affected during REM than non-REM (Fig. 2A, D; significant genotype by sleep stage interaction effects: F(3,168) = 35.7, p < 0.001 for time spent in sleep and F(3,169) = 23.1, p < 0.001 for number of sleep bouts). *Ank3-1b* deletion did not affect the duration of NREM sleep epochs (Fig. 2A; no significant main effect of genotype on sleep duration: F(2,85) = 1.6, p = 0.20), although the number of NREM bouts per hour was significantly lower in *Ank3-1b*$^{KO/KO}$ mice than in wildtype mice (significant main effect of genotype: F(2,85) = 5.6, p = 0.005; *Ank3-1b*$^{KO/KO}$ vs wildtype: t(85) = 3.4, p = 0.004; other pairwise comparisons were non-significant). In contrast, the duration of sleep epochs during REM was significantly lower in *Ank3-1b* KO mice than in wildtype mice (Fig. 2D; main effect of genotype on sleep duration: F(2,84) = 6.8, p = 0.002; post-hoc pairwise comparisons: *Ank3-1b*$^{KO/KO}$ vs wildtype: t(84) = 2.5, p = 0.03; *Ank3-1b*$^{KO/+}$ vs wildtype: t(84) = 3.6, p = 0.002). The number of REM bouts per hour was also significantly lower in *Ank3-1b* KO mice than in wildtype mice (Fig. 2D; main effect of genotype on number of sleep bouts: F(2,84) = 13.5, p < 0.001; post-hoc pairwise comparisons: *Ank3-1b*$^{KO/KO}$ vs wildtype: t(84) = 5.1, p < 0.001; *Ank3-1b*$^{KO/+}$ vs wildtype: t(84) = 3.4, p = 0.002). These findings suggest that *Ank3-1b* deletion more strongly disrupts REM sleep than NREM sleep. It is important to note that due to lack of simultaneous electromyography (EMG) recordings, we were unable to definitively determine if overall REM time and number of REM bouts was reduced, or if this data simply reflects disruption of normal theta-delta ratios characteristic of classic REM sleep. Nonetheless, disrupted REM properties are indicative of many different sleep disorders and are implicated in BD[35–42]. These data warrant further investigation of sleep deficits in this model, which stands to provide important insights and implications for BD treatments.

We next examined whether disturbances in REM and NREM sleep patterns were accompanied by disturbances in EEG rhythms during sleep. We found that *Ank3-1b* deletion affected oscillatory power differently during REM and NREM sleep (generalized linear mixed model: significant genotype by sleep stage interaction: $F(3,342) = 92.3$, $p < 0.001$; significant genotype by sleep stage by rhythm type interaction: $F(12,342) = 1178.1$, $p < 0.001$), with stronger effects of *Ank3-1b* deletion on power spectra observed during REM than NREM (Fig. 2B, E). Therefore, we next analyzed EEG rhythms during NREM and REM separately.

During identified NREM sleep epochs, *Ank3-1b* deletion did not produce generalized effects on power across all frequencies (generalized linear mixed model: significant genotype by rhythm type interaction: $F(6,168) = 53.7$, $p < 0.001$). Instead, effects of *Ank3-1b* deletion on rhythmic power were most pronounced for slow gamma rhythms (Fig. 2B). Slow gamma power was significantly greater in *Ank3-1b* KO mice than in wildtype mice in a gene-dosage dependent manner (Fig. 2C; main effect of genotype on slow gamma power: $F(2,56) = 38.5$, $p < 0.001$; post-hoc pairwise comparisons: *Ank3-1b*$^{KO/KO}$ vs wildtype slow gamma: $t(56) = 8.8$, $p < 0.001$; *Ank3-1b*$^{KO/+}$ vs wildtype slow gamma: $t(56) = 3.5$, $p = 0.001$; *Ank3-1b*$^{KO/KO}$ vs *Ank3-1b*$^{KO/+}$: $t(56) = 7.0$, $p < 0.001$). *Ank3-1b* deletion also modestly affected delta rhythms, a type of rhythm that is predominant in EEG recordings during NREM[43]. However, in contrast to gamma results, power in the delta frequency range was significantly lower in homozygous KOs than in wildtype mice (generalized linear mixed model: main effect of genotype on delta power during NREM: $F(2,56) = 5.5$, $p = 0.007$; post-hoc pairwise comparisons: *Ank3-1b*$^{KO/KO}$ vs wildtype delta: $t(56) = 2.4$, $p = 0.04$; *Ank3-1b*$^{KO/+}$ vs wildtype delta: $t(56) = 1.0$, $p = 0.34$) and significantly lower in homozygous KOs than in heterozygous KOs (*Ank3-1b*$^{KO/KO}$ vs *Ank3-1b*$^{KO/KO}$: $t(56) = 3.3$, $p = 0.005$).

We next investigated how *Ank3-1b* deletion altered EEG rhythms during identified REM sleep epochs. We again assessed slow gamma rhythms and also assessed theta, a rhythm type that dominates EEG recordings during REM sleep[43]. *Ank3-1b* deletion differentially affected the power of the different rhythm types during REM (Fig. 2E; generalized linear mixed model: significant genotype by rhythm type interaction: $F(6,174) = 2302.5$, $p < 0.001$). The power of slow gamma rhythms during REM significantly differed across genotypes (Fig. 2F, main effect of genotype: $F(2,58) = 404.0$, $p < 0.001$). Specifically, slow gamma power increased with decreasing levels of *Ank3-1b* (post-hoc pairwise comparisons: wildtype vs *Ank3-1b*$^{KO/+}$ slow gamma: $t(58) = 2.5$, $p = 0.02$; *Ank3-1b*$^{KO/+}$ vs *Ank3-1b*$^{KO/KO}$ slow gamma: $t(58) = 21.6$, $p < 0.001$; *Ank3-1b*$^{KO/KO}$ vs wildtype slow gamma: $t(58) = 27.3$, $p < 0.001$). Theta power during REM also significantly differed across genotypes (main effect of genotype: $F(2,58) = 94.8$, $p < 0.001$). However, in contrast to slow gamma results, homozygous *Ank3-1b* deletion significantly decreased theta power during REM (post-hoc pairwise comparisons: *Ank3-1b*$^{KO/KO}$ vs wildtype theta: $t(58) = 6.2$, $p < 0.001$). Also, theta power during REM did not significantly differ between wildtype mice and heterozygous KOs (wildtype vs *Ank3-1b*$^{KO/+}$ theta: $t(58) = 1.9$, $p = 0.07$). Taken together, this collection of results suggests a potential relationship between increased slow gamma power and disrupted REM sleep.

Previous characterization of these mice showed that *Ank3-1b*$^{KO/KO}$ mice have premature mortality rates[16], and meet the criteria for sudden death in epilepsy (SUDEP), so we also looked at seizure activity during REM and NREM sleep. Our data indicates that seizures are approximately 10X more common during REM (1.24 seizures/hr) than during NREM (0.13 seizures/hr) sleep, and this increased seizure frequency was statistically significant in REM (n = 9, mean rank = 12.11) compared to NREM sleep (n = 9, mean rank = 6.89; p = 0.040, std error = ± 9.957; Supplementary Fig. 4A & B). This result was striking because seizures triggered during REM sleep are more likely to cause sudden death compared to other times of the day and NREM sleep.[44] Then we looked at the effects of seizure occurrence on gamma power in *Ank3-1b*$^{KO/+}$ and *Ank3-1b*$^{KO/KO}$ mice and found that seizure occurrence affected gamma power differently between genotypes during REM sleep (generalized linear mixed model: significant genotype by seizure occurrence interaction: $F(2,38) = 15.3$, $p < 0.001$). We found that seizure occurrence had no significant effect on gamma power in *Ank3-1b*$^{KO/+}$ (seizure occurrence vs. no seizure occurrence: $F(1,19) = 0.5$; $t(19) = 0.7$, $p = 0.5$), but seizure occurrence was associated with significantly increased gamma power in *Ank3-1b*$^{KO/KO}$ mice (seizure occurrence vs. no seizure occurrence: $F(1,19) = 404$; $t(19) = 20.1$, $p < 0.001$; Supplementary Fig. 4C). This highlights again a positive correlation between seizure phenotype severity and increased slow gamma power and suggests that seizure activity and slow gamma rhythms may be associated. When we looked at the effect of seizure occurrence on theta power in *Ank3-1b*$^{KO/+}$ and *Ank3-1b*$^{KO/KO}$ mice during REM sleep, we found that seizure occurrence affected theta power differently between genotypes (significant genotype by seizure occurrence interaction: $F(2,38) = 114.7$, $p < 0.001$). We found that seizure occurrence had no significant effect on theta power in *Ank3-1b*$^{KO/+}$ (seizure occurrence vs. no seizure occurrence: $F(1,19) = 4.1$; $t(19) = 2.0$, $p = 0.06$), but seizure occurrence was associated with significantly decrease theta power in *Ank3-1b*$^{KO/KO}$ mice (seizure occurrence vs. no seizure occurrence: $F(1,19) = 228.5$; $t(19) = 15.1$, $p < 0.001$; Supplementary Fig. 4D). Seizures were extremely rare during NREM; only a single mouse exhibited seizures during NREM. Thus, we were unable to explore potential differential effects of seizure occurrence on gamma power during NREM.

Again, it is important to note that seizures may be unaccounted for due to potentially unidentified sleep bouts, since thorough analysis of sleep requires simultaneous EMG analysis. Mice may be having seizures during REM and NREM periods that our algorithm was unable to identify due to disrupted theta-delta-ratios. Thus, it is critical for future studies to further explore these effects in order to better understand the risk and underlying mechanisms leading to SWDs during sleep in this model. This connection between disrupted REM sleep and increased epileptic activity is another shared feature of the *Ank3* link to bipolar disorder and epilepsy.

Ank3-1b **KO mice exhibit hyperactivity during awake behaviors**

Since activity levels are altered in depressive and manic states of BD, we looked at awake rest and walking behaviors in *Ank3* KO mice (Fig. 3A, D). Awake rest and walking behaviors were classified using LDA on the kinematic information from the videos taken for bouts lasting longer than 0.5 seconds. Awake rest states were defined as periods during which the mouse was not moving but was not identified

as asleep by the sleep classifier. The number of awake rest (Fig. 3A) and walking (Fig. 3B) bouts per hour were differentially affected by *Ank3-1b* deletion (significant genotype by behavior type interaction: F(2,168) = 4.8, p = 0.001). Compared to wildtype mice, *Ank3-1b*$^{KO/KO}$ mice exhibited significantly fewer bouts of awake rest per hour (generalized linear mixed model, significant main effect of genotype: F(2,84) = 5.4, p = 0.006; post-hoc pairwise comparisons: wildtype vs *Ank3-1b*$^{KO/+}$: t(84) = 2.2, p = 0.07; *Ank3-1b*$^{KO/KO}$ vs *Ank3-1b*$^{KO/+}$: t(84) = 0.9, p = 0.4; *Ank3-1b*$^{KO/KO}$ vs wildtype: t(84) = 3.2, p = 0.006) and spent less time (minutes per hour) in the awake rest state (Fig. 3A, significant main effect of genotype: F(2,84) = 3.9, p = 0.002; post-hoc pairwise comparisons: wildtype vs *Ank3-1b*$^{KO/+}$: t(84) = 2.1, p = 0.7; *Ank3-1b*$^{KO/KO}$ vs *Ank3-1b*$^{KO/+}$: t(84) = 0.2, p = 0.9; *Ank3-1b*$^{KO/KO}$ vs wildtype: t(84) = 2.6, p = 0.04). Regarding walking behavior, significantly more walking bouts per hour were observed for *Ank3-1b* KO mice compared to wildtype mice (Fig. 3D; significant main effect of genotype: F(2,84) = 12.8, p < 0.001; post-hoc pairwise comparisons: wildtype vs *Ank3-1b*$^{KO/+}$: t(84) = 4.9, p < 0.001; *Ank3-1b*$^{KO/KO}$ vs wildtype: t(84) = 3.4, p = 0.002). Also, *Ank3-1b* KO mice spent significantly more time walking compared to wildtype mice (Fig. 3D; significant main effect of genotype: F(2,84) = 8.6, p < 0.001; post-hoc pairwise comparisons: *Ank3-1b*$^{KO/KO}$ vs wildtype: t(84) = 3.2, p = 0.04; *Ank3-1b*$^{KO/+}$ vs wildtype: t(84) = 4.1, p < 0.001). These data support the claim for a manic-like phenotype in *Ank3-1b* KO mice previously reported[26].

Ank3-1b **KO mice exhibit increased slow gamma power during awake rest and walking states**

Delta rhythms are often evident during periods of awake rest in rodents[45–47], and low frequency theta can be associated with non-moving states[48]. Therefore, we included measurements of these rhythm types, together with slow gamma rhythms, in our model when testing for differences in the power of EEG rhythms between genotypes during awake rest. During awake rest, the different rhythm types were differentially affected by *Ank3-1b* deletion, with largest effects observed for slow gamma rhythms (Fig. 3B, generalized linear mixed model, significant genotype by rhythm type interaction effect: (F(6,159) = 173.8, p < 0.001). Slow gamma power increased as *Ank3-1b* levels decreased across the three genotypes (Fig. 3C, significant main effect of genotype: F(2,53) = 94.0, p < 0.001). *Ank3-1b*$^{KO/KO}$ and *Ank3-1b*$^{KO/+}$ mice had significantly increased slow gamma power compared to wildtype mice, and *Ank3-1b*$^{KO/KO}$ mice had significantly higher slow gamma than *Ank3-1b*$^{KO/+}$ mice (post-hoc pairwise comparisons: wildtype vs *Ank3-1b*$^{KO/+}$: t(53) = 8.4, p < 0.001; *Ank3-1b*$^{KO/KO}$ vs *Ank3-1b*$^{KO/+}$: t(53) = 7.2, p < 0.001; *Ank3-1b*$^{KO/KO}$ vs wildtype: t(53) = 12.8, p < 0.001). In contrast, power in the theta frequency range was not significantly affected by *Ank3-1b* deletion (no significant main effect of genotype on theta power: F(2,53) = 1.7, p = 0.2), and delta power was lower in *Ank3-1b*$^{KO/KO}$ mice than in wildtype mice (significant main effect of genotype: F(2,53) = 67.8, p < 0.001; post-hoc pairwise comparison: *Ank3-1b*$^{KO/KO}$ vs wildtype: t(53) = 3.2, p < 0.005).

We next assessed the effects of *Ank3-1b* deletion on EEG rhythms during walking behavior. Active walking behavior is associated with prominent theta and gamma activity in local field potential recordings from rodents[49–51]. Thus, during walking, we tested for theta and slow gamma power

differences across genotypes. We found that theta and slow gamma rhythms during walking were differentially affected by *Ank3-1b* deletion (generalized linear mixed model, significant genotype by rhythm type interaction effect: $F(3,112) = 75.5$, $p < 0.001$). Slow gamma rhythms during walking were significantly increased by *Ank3-1b* deletion (Fig. 3F, significant main effect of genotype on slow gamma: $F(2,56) = 189.3$, $p < 0.001$). As was observed during awake rest, slow gamma power increased with decreasing *Ank3-1b* (post-hoc pairwise comparisons: wildtype vs *Ank3-1b*$^{KO/+}$: $t(56) = 4.9$, $p < 0.001$; *Ank3-1b*$^{KO/KO}$ vs *Ank3-1b*$^{KO/+}$: $t(56) = 13.2$, $p < 0.001$; *Ank3-1b*$^{KO/KO}$ vs wildtype: $t(56) = 18.9$, $p < 0.001$). In contrast, theta power during walking was significantly decreased in *Ank3-1b* knockout mice compared to wildtype mice (significant main effect of genotype: $F(2,56) = 56.8$, $p < 0.001$; post-hoc pairwise comparisons: wildtype vs *Ank3-1b*$^{KO/+}$: $t(56) = 9.4$, $p < 0.001$; *Ank3-1b*$^{KO/KO}$ vs wildtype: $t(56) = 9.2$, $p < 0.001$).

Ank3-1b **KO mice exhibit increases in repetitive behaviors**

Another endophenotype of BD is obsessive and compulsive thoughts and behaviors[52,53]. One way to test for such characteristics in mice is to look at their propensity for repetitive behaviors, such as repetitive grooming and digging. Repetitive behaviors are another characteristic related to BD that has not previously been explored in *Ank3-1b* mice. Thus, we compared the frequency of grooming and digging behaviors in *Ank3-1b* KO and wildtype mice. We found a significant effect of *Ank3-1b* deletion on repetitive grooming bouts and amount of time spent grooming per hour (Fig. 4A; generalized linear mixed model, main effect on genotype: bouts: $F(2,84) = 36.3$, $p < 0.001$; time: $F(2,84) = 44.5$, $p < 0.001$). However, only heterozygous but not homozygous *Ank3-1b* deletion significantly altered grooming bouts (post-hoc pairwise comparisons: wildtype vs *Ank3-1b*$^{KO/+}$: $t(84) = 7.4$, $p < 0.001$; *Ank3-1b*$^{KO/KO}$ vs *Ank3-1b*$^{KO/+}$: $t(84) = 7.6$, $p < 0.001$; *Ank3-1b*$^{KO/KO}$ vs wildtype: $t(84) = 0.05$, $p = 1.0$). Also, only heterozygous but not homozygous *Ank3-1b* KO mice showed significantly increased time grooming (generalized linear mixed model, main effect on genotype: wildtype vs *Ank3-1b*$^{KO/+}$: $t(84) = 8.7$, $p < 0.001$; *Ank3-1b*$^{KO/KO}$ vs *Ank3-1b*$^{KO/+}$: $t(84) = 8.1$, $p < 0.001$; *Ank3-1b*$^{KO/KO}$ vs wildtype: $t(84) = 0.7$, $p = 0.5$). Digging may provide a better measure of repetitive behaviors in *Ank3-1b* mice because, unlike grooming, it does not require animals to balance on their hind paws which may be more difficult for *Ank3-1b*$^{KO/KO}$ mice due to their mild ataxia. A significant effect of *Ank3-1b* deletion on digging behaviors was observed (Fig. 4D) when digging was measured in bouts per hour (generalized linear mixed model, main effect of genotype: $F(2,84) = 6.6$, $p = 0.002$). As was the case with grooming, only heterozygous *Ank3-1b* KO mice and not homozygous *Ank3-1b* KO mice showed significantly more digging bouts per hour in compared to wildtype mice (post-hoc pairwise comparisons: wildtype vs *Ank3-1b*$^{KO/+}$: $t(84) = 3.6$, $p = 0.002$; *Ank3-1b*$^{KO/KO}$ vs *Ank3-1b*$^{KO/+}$: $t(84) = 2.5$, $p = 0.03$; *Ank3-1b*$^{KO/KO}$ vs wildtype: $t(84) = 1.3$, $p = 0.21$). We also found a significant effect of *Ank3-1b* deletion on repetitive digging minutes per hour (generalized linear mixed model, main effect on genotype: $F(2,84) = 5.5$, $p = 0.006$). Unlike with grooming, both heterozygous *Ank3-1b* KO mice and homozygous *Ank3-1b* KO mice showed significantly increased digging time compared to wildtype mice (generalized linear mixed model, main effect on genotype: wildtype vs *Ank3-1b*$^{KO/+}$: $t(84) = 2.8$, $p = 0.02$;

Ank3-1b$^{KO/KO}$ vs *Ank3-1b*$^{KO/+}$: t(84) = 0.2, p = 0.9; *Ank3-1b*$^{KO/KO}$ vs wildtype: t(84) = 2.9, p = 0.02). It is interesting to note that while one would expect the magnitude of behavioral effects to increase with reduced *Ank3-1b* dosage, *Ank3-1b*$^{KO/+}$ mice exhibited the strongest repetitive behaviors phenotype. This may be due to the confounding factor of ataxia in *Ank3-1b*$^{KO/KO}$ mice[27], making it difficult for *Ank3-1b*$^{KO/KO}$ mice to engage in prolonged bouts of coordinated grooming and digging movements.

Ank3-1b KO mice show increased slow gamma rhythms during repetitive behaviors

Power spectra during grooming behaviors showed peaks in the theta and slow gamma bands, so we next examined whether *Ank3-1b* deletion affected theta and slow gamma power during grooming. As was observed for other awake behaviors, different effects of *Ank3-1b* deletion on theta and slow gamma power were observed during grooming behaviors (Fig. 4B, generalized linear mixed models, significant genotype by rhythm type interaction effect on grooming behaviors: F(3,136) = 114.8, p < 0.001). Specifically, slow gamma power was increased by *Ank3-1b* deletion in a dosage-dependent manner (Fig. 4C, generalized linear mixed model, significant main effect of genotype: F(2,60) = 59.6, p < 0.001; post-hoc pairwise comparisons: wildtype vs *Ank3-1b*$^{KO/+}$: t(60) = 3.8, p < 0.001; *Ank3-1b*$^{KO/+}$ vs *Ank3-1b*$^{KO/KO}$: t(60) = 7.6, p < 0.001; *Ank3-1b*$^{KO/KO}$ vs wildtype: t(60) = 10.8, p < 0.001). In contrast, *Ank3-1b* deletion decreased theta power (generalized linear mixed model, significant main effect of genotype: F(2,60) = 5.3, p = 0.008), but the only post-hoc pairwise comparison that was significantly different was the comparison of theta power in *Ank3-1b*$^{KO/+}$ mice and wildtype mice (t(60) = 3.2, p = 0.006). Similar to slow gamma power during grooming, slow gamma power during digging was increased by *Ank3-1b* deletion in a dosage-dependent manner (Fig. 4E-F, generalized linear mixed model, significant main effect of genotype: F(2,68) = 118.2, p < 0.001; post-hoc pairwise comparisons: wildtype vs *Ank3-1b*$^{KO/+}$: t(68) = 5.8, p < 0.001; *Ank3-1b*$^{KO/+}$ vs *Ank3-1b*$^{KO/KO}$: t(68) = 10.0, p < 0.001; *Ank3-1b*$^{KO/KO}$ vs wildtype: t(68) = 15.4, p < 0.001). Indeed, analyses revealed that *Ank3-1b* deletion affected slow gamma power similarly during the different types of repetitive behaviors (i.e., grooming and digging; generalized linear mixed model, no significant main effect of repetitive behavior type on slow gamma power: F(1,128) = 0.41, p = 0.525; no significant genotype by repetitive behavior type interaction effect: F(1, 128) = 0.27, p = 0.76). Therefore, we included slow gamma measurements from grooming and digging behaviors together and again assessed the effect of *Ank3-1b* deletion on slow gamma rhythm power. As was observed for grooming and digging behaviors alone, *Ank3-1b* deletion increased slow gamma power during grooming and digging behaviors analyzed together (generalized linear mixed model, main effect of genotype: F(2,128) = 91.9, p < 0.001). During grooming and digging behaviors, slow gamma power in both *Ank3-1b*$^{KO/+}$ and *Ank3-1b*$^{KO/KO}$ mice was larger than slow gamma power in wildtype mice (post-hoc pairwise comparisons: wildtype vs *Ank3-1b*$^{KO/+}$: t(128) = 3.9, p < 0.001; *Ank3-1b*$^{KO/KO}$ vs wildtype: t(128) = 13.2, p < 0.001). Also, slow gamma power during grooming and digging behaviors was greater in homozygous KO mice than in heterozygous KO mice (*Ank3-1b*$^{KO/+}$ vs *Ank3-1b*$^{KO/KO}$: t(128) = 9.7, p < 0.001). Taken together, these findings suggest that increased slow gamma rhythms accompany increased repetitive behaviors in the *Ank3-1b* mice. Interestingly, increased gamma power (20–50 Hz) has been shown to be associated with

repetitive behaviors in autism spectrum disorder (ASD) patients[54], and ANK3 rare variants have been found in patients with ASD[55–57]. Thus, not only is this phenotype in *Ank3-1b* mice relevant for BD, but it may also have implications for ASD.

DISCUSSION

Human genetic studies have advanced our understanding of psychiatric illness through the identification of rare and common variants associated with complex neurodevelopmental disorders. However, understanding the role that such variants play in polygenic traits like those symptomatic of BD has remained a challenge. One such challenge is the difficulty of modeling subjective human traits like mood in rodents. Even more difficult is modeling a cyclic disorder like BD that is characterized by extreme shifts in mood lasting on a time scale of weeks to months.

Many studies attempting to utilize *Ank3* as a model of BD in mice have shown promise. For example, one study showed that *Ank3-1b*$^{KO/+}$ mice model aspects of BD such as shifts from manic-like features including reduced anxiety and increased motivation for reward, to depressive-like features after chronic stress that was attenuated by lithium[26]. However, these behaviors were of small effect size and difficult to reproduce in small scale studies. Alternatively, a pyramidal cell forebrain conditional KO of *Ank3* exhibited similar behavioral phenotypes modeling BD but with greater effect size[58]. In this model, behaviors at baseline were manic-like, including hyperactivity, and changed to depressive-like features after social defeat stress. This phenotype was also attenuated by lithium and valproate. However, the genetic manipulation was more severe than the diminished ANK3 expression reported in human studies, and neither study modeled the full range of BD symptoms and endophenotypes.

These limitations illustrate the trade-off that exists between models with BD-related phenotypes of large effect size and those that more accurately model BD variable expressivity but have phenotypes of smaller effect size. This trade-off affects overall reproducibility in rodent experiments and their translational relevance to BD treatment in human patients. Our approach was able to identify new BD-related behaviors in *Ank3-1b* mice and provides advanced methodology that can be tailored towards long-term behavioral analysis of mice. We developed algorithms suitable for analyzing long term undisturbed home cage activity that more faithfully captures behavioral rhythmicity seen in BD.

Furthermore, our results illustrate a robust behavioral and electrophysiological phenotype that can be used for future in vivo single unit electrophysiological experiments conducted over periods of weeks to months with the intention of gaining mechanistic insights into behaviors relevant to BD symptoms seen in human patients. For example, the sleep disturbance phenotype that we have identified in this model has direct relevance to patient treatment of BD because sleep disturbances are present across all states of BD and highly consequential for treatment[59]. While manic states of BD are characterized by decreased need for sleep and depressive states of BD are characterized by increased sleep, even euthymic states of BD show characteristics of sleep disturbance[35–42]. The most consistent result across mood states of BD is increased REM density and sleep latency.

Recently, a quantitative phosphoproteomic study has implicated *Ank3* in sleep need, lending support to our findings of dysregulated sleep in *Ank3-1b* KO mice[60]. Future studies utilizing EMG will be helpful for studying specific types of REM disturbances in *Ank3-1b* mice and further understanding the role of *Ank3-1b* in sleep need. Interestingly, there is growing evidence for a role of REM sleep in emotional memory processing in the hippocampus[61–64], and gamma is thought to promote memory consolidation during REM sleep[65]. Additionally, our data is consistent with phenotypes seen in the Kv3.1/Kv3.3 mouse model. Like to *Ank3*, Kv3-type channels are expressed in interneurons, and Kv3.1 is expressed only in PV-interneurons. Deletion of Kv3.1/Kv3.3 in PV-interneurons leads to decreased action potential hyperactivity and increased slow gamma power (20–60 Hz)[66–69].

Given previous studies showed reduced PV-interneuron firing rates in ranges above 100 Hz in *Ank3-1b*$^{KO/KO}$ mice[16], we hypothesize that the increased slow gamma power seen here was due to an inability of PV-interneurons in KO mice to fire at frequencies high enough to produce fast gamma oscillations. Since PV-interneurons in the cortex and hippocampus have been shown to be more active during REM than NREM in the cortex and hippocampus[70], this could explain why we see a bigger effect of *Ank3-1b* loss on REM sleep compared to NREM sleep, and why seizures are more common during REM sleep in this model. Furthermore, we hypothesize that the increased slow gamma seen during other behavioral states may have to do with changes in behavior that we were not able to identify here due to limitations of the existing dataset such as limited recording durations, camera angles for distinguishes more complex behaviors, sample size, and EEG sampling frequency.

Further studies examining the relationship between the increases in slow gamma power observed here, and changes in power of other frequency bands, with changes in *Ank3-1b* KO mice behavior will be important for understanding the human relevance of these mice as a model of BD. For example, theta-gamma coupling is highly implicated in processes of memory and navigation in both humans and rodents[71], and gamma coherence is disrupted during various tasks in human subjects with BD[22,72]. Studies of gamma in BD have shown increased power in the 30–50 Hz range in BD patients during visual tasks and resting states[23,24,73]. This increased slow gamma phenotype in *Ank3-1b* KO mice may present another way in which EEG disturbances can be used in translational studies to develop treatments for patients with BD.

Declarations

ACKNOWLEDGEMENTS

The authors acknowledge the Texas Advanced Computing Center (TACC) at The University of Texas at Austin for providing high performance computing resources that have contributed to the research results reported within this paper. URL: http://www.tacc.utexas.edu. We would also like to acknowledge Uzair Saleem for his help manually verifying some of the automated video data analysis. We would also like to thank Cory Massey for access to video-EEG recordings performed in the Noebels lab. We would also like

to especially acknowledge the generosity and support of Dr. Edward C. Cooper, under whose guidance, mentorship, and funding (NIH R01 NS49119) the original data was collected at Baylor College of Medicine. This work was supported by: American Physiological Society Hearst Summer Undergraduate Research Fellowship (to N.R.), The Neuroscience Studies Foundation in Honor of Harvey and Judi Nudelman Neuroscience and Neurology Summer Internship and Nudelman Pioneer Award (to S.K.), NSF CAREER Award 1453756 (to L.L.C.), and UT Austin Provost's Early Career Fellowship (to A.Y.L.).

References

1. Tondo, L., Pompili, M., Forte, A. & Baldessarini, R. J. Suicide attempts in bipolar disorders: comprehensive review of 101 reports. Acta Psychiatrica Scandinavica **133**, 174–186, doi:https://doi.org/10.1111/acps.12517 (2016).
2. Toma, C. *et al.* A linkage and exome study of multiplex families with bipolar disorder implicates rare coding variants of ANK3 and additional rare alleles at 10q11-q21. J Psychiatry Neurosci **46**, E247-e257, doi:10.1503/jpn.200083 (2021).
3. Nelson, A. D. *et al.* Ankyrin-G regulates forebrain connectivity and network synchronization via interaction with GABARAP. Mol Psychiatry **25**, 2800–2817, doi:10.1038/s41380-018-0308-x (2020).
4. Farwell, K. D. *et al.* Enhanced utility of family-centered diagnostic exome sequencing with inheritance model-based analysis: results from 500 unselected families with undiagnosed genetic conditions. Genet Med **17**, 578–586, doi:10.1038/gim.2014.154 (2015).
5. Ferreira, M. A. *et al.* Collaborative genome-wide association analysis supports a role for ANK3 and CACNA1C in bipolar disorder. Nat Genet **40**, 1056–1058, doi:10.1038/ng.209 (2008).
6. Schulze, T. G. *et al.* Two variants in Ankyrin 3 (ANK3) are independent genetic risk factors for bipolar disorder. Mol Psychiatry **14**, 487–491, doi:10.1038/mp.2008.134 (2009).
7. Scott, L. J. *et al.* Genome-wide association and meta-analysis of bipolar disorder in individuals of European ancestry. Proc Natl Acad Sci U S A **106**, 7501–7506, doi:10.1073/pnas.0813386106 (2009).
8. Tesli, M. *et al.* Association analysis of ANK3 gene variants in nordic bipolar disorder and schizophrenia case-control samples. *Am J Med Genet B Neuropsychiatr Genet* **156b**, 969–974, doi:10.1002/ajmg.b.31244 (2011).
9. Consortium, T. S. P. G.-W. A. S. G. Genome-wide association study identifies five new schizophrenia loci. Nat Genet **43**, 969–976, doi:10.1038/ng.940 (2011).
10. Mühleisen, T. W. *et al.* Genome-wide association study reveals two new risk loci for bipolar disorder. Nat Commun **5**, 3339, doi:10.1038/ncomms4339 (2014).
11. Rueckert, E. H. *et al.* Cis-acting regulation of brain-specific ANK3 gene expression by a genetic variant associated with bipolar disorder. Mol Psychiatry **18**, 922–929, doi:10.1038/mp.2012.104 (2013).
12. Wirgenes, K. V. *et al.* ANK3 gene expression in bipolar disorder and schizophrenia. Br J Psychiatry **205**, 244–245, doi:10.1192/bjp.bp.114.145433 (2014).

13. Tang, L. *et al.* ANK3 Gene Polymorphism Rs10994336 Influences Executive Functions by Modulating Methylation in Patients With Bipolar Disorder. Front Neurosci **15**, 682873, doi:10.3389/fnins.2021.682873 (2021).
14. Nelson, A. D. & Jenkins, P. M. The splice is right: ANK3 and the control of cortical circuits. Biological psychiatry **80**, 263–265 (2016).
15. Xu, M. & Cooper, E. C. An Ankyrin-G N-terminal Gate and Protein Kinase CK2 Dually Regulate Binding of Voltage-gated Sodium and KCNQ2/3 Potassium Channels. J Biol Chem **290**, 16619–16632, doi:10.1074/jbc.M115.638932 (2015).
16. Lopez, A. Y. *et al.* Ankyrin-G isoform imbalance and interneuronopathy link epilepsy and bipolar disorder. Mol Psychiatry **22**, 1464–1472, doi:10.1038/mp.2016.233 (2017).
17. Hesdorffer, D. C. *et al.* Epilepsy, suicidality, and psychiatric disorders: a bidirectional association. Ann Neurol **72**, 184–191, doi:10.1002/ana.23601 (2012).
18. García-Morales, I., de la Peña Mayor, P. & Kanner, A. M. Psychiatric comorbidities in epilepsy: identification and treatment. Neurologist **14**, S15–25, doi:10.1097/01.nrl.0000340788.07672.51 (2008).
19. Wotton, C. J. & Goldacre, M. J. Record-linkage studies of the coexistence of epilepsy and bipolar disorder. Soc Psychiatry Psychiatr Epidemiol **49**, 1483–1488, doi:10.1007/s00127-014-0853-9 (2014).
20. Toker, L., Mancarci, B. O., Tripathy, S. & Pavlidis, P. Transcriptomic Evidence for Alterations in Astrocytes and Parvalbumin Interneurons in Subjects With Bipolar Disorder and Schizophrenia. Biological Psychiatry **84**, 787–796, doi:https://doi.org/10.1016/j.biopsych.2018.07.010 (2018).
21. Steullet, P. *et al.* The thalamic reticular nucleus in schizophrenia and bipolar disorder: role of parvalbumin-expressing neuron networks and oxidative stress. Molecular Psychiatry **23**, 2057–2065, doi:10.1038/mp.2017.230 (2018).
22. Özerdem, A., Güntekin, B., Atagün, I., Turp, B. & Başar, E. Reduced long distance gamma (28–48 Hz) coherence in euthymic patients with bipolar disorder. J Affect Disord **132**, 325–332, doi:10.1016/j.jad.2011.02.028 (2011).
23. Liu, T. Y., Chen, Y. S., Su, T. P., Hsieh, J. C. & Chen, L. F. Abnormal early gamma responses to emotional faces differentiate unipolar from bipolar disorder patients. *Biomed Res Int* 2014, 906104, doi:10.1155/2014/906104 (2014).
24. Benjamín Cea-Cañas, Á. D., Alba Lubeiro, María Iglesias, Carmen Capella, Alberto Rodríguez-Lorenzana, Vicente Molina. Altered gamma band noise power in schizophrenia and bipolar patients during a cognitive task. The European Journal of Psychiatry **35**, doi:https://doi.org/10.1016/j.ejpsy.2020.11.003 (2021).
25. Hu, H., Gan, J. & Jonas, P. Fast-spiking, parvalbumin < sup>+</sup > GABAergic interneurons: From cellular design to microcircuit function. Science **345**, 1255263, doi:doi:10.1126/science.1255263 (2014).

26. Leussis, M. P. *et al.* The ANK3 bipolar disorder gene regulates psychiatric-related behaviors that are modulated by lithium and stress. Biol Psychiatry **73**, 683–690, doi:10.1016/j.biopsych.2012.10.016 (2013).
27. Zhou, D. *et al.* AnkyrinG is required for clustering of voltage-gated Na channels at axon initial segments and for normal action potential firing. J Cell Biol **143**, 1295–1304, doi:10.1083/jcb.143.5.1295 (1998).
28. Mathis, A. *et al.* DeepLabCut: markerless pose estimation of user-defined body parts with deep learning. Nat Neurosci **21**, 1281–1289, doi:10.1038/s41593-018-0209-y (2018).
29. Singh, S., Bermudez-Contreras, E., Nazari, M., Sutherland, R. J. & Mohajerani, M. H. Low-cost solution for rodent home-cage behaviour monitoring. PLoS One **14**, e0220751, doi:10.1371/journal.pone.0220751 (2019).
30. Pfammatter, J. A., Maganti, R. K. & Jones, M. V. An automated, machine learning-based detection algorithm for spike-wave discharges (SWDs) in a mouse model of absence epilepsy. Epilepsia Open **4**, 110–122, doi:10.1002/epi4.12303 (2019).
31. Tallon-Baudry, C., Bertrand, O., Delpuech, C. & Pernier, J. Oscillatory γ-Band (30–70 Hz) Activity Induced by a Visual Search Task in Humans. The Journal of Neuroscience **17**, 722–734, doi:10.1523/jneurosci.17-02-00722.1997 (1997).
32. Colgin, L. L. *et al.* Frequency of gamma oscillations routes flow of information in the hippocampus. Nature **462**, 353–357, doi:10.1038/nature08573 (2009).
33. Trettel, S. G., Trimper, J. B., Hwaun, E., Fiete, I. R. & Colgin, L. L. Grid cell co-activity patterns during sleep reflect spatial overlap of grid fields during active behaviors. Nat Neurosci **22**, 609–617, doi:10.1038/s41593-019-0359-6 (2019).
34. Csicsvari, J., Hirase, H., Czurkó, A., Mamiya, A. & Buzsáki, G. Fast network oscillations in the hippocampal CA1 region of the behaving rat. *J Neurosci* **19**, Rc20, doi:10.1523/JNEUROSCI.19-16-j0001.1999 (1999).
35. Duncan, W. C., Jr., Pettigrew, K. D. & Gillin, J. C. REM architecture changes in bipolar and unipolar depression. Am J Psychiatry **136**, 1424–1427, doi:10.1176/ajp.136.11.1424 (1979).
36. Wehr, T. A., Wirz-Justice, A., Goodwin, F. K., Duncan, W. & Gillin, J. C. Phase advance of the circadian sleep-wake cycle as an antidepressant. Science **206**, 710–713, doi:10.1126/science.227056 (1979).
37. Giles, D. E., Rush, A. J. & Roffwarg, H. P. Sleep parameters in bipolar I, bipolar II, and unipolar depressions. Biol Psychiatry **21**, 1340–1343, doi:10.1016/0006-3223(86)90319-7 (1986).
38. de Maertelaer, V., Hoffman, G., Lemaire, M. & Mendlewicz, J. Sleep spindle activity changes in patients with affective disorders. Sleep **10**, 443–451, doi:10.1093/sleep/10.5.443 (1987).
39. Hudson, J. I. *et al.* Polysomnographic Characteristics of Young Manic Patients: Comparison With Unipolar Depressed Patients and Normal Control Subjects. Archives of General Psychiatry **49**, 378–383, doi:10.1001/archpsyc.1992.01820050042006 (1992).
40. Fossion, P. *et al.* Does sleep EEG data distinguish between UP, BPI or BPII major depressions? An age and gender controlled study. J Affect Disord **49**, 181–187, doi:10.1016/s0165-0327(97)00111-0

(1998).

41. Riemann, D., Voderholzer, U. & Berger, M. Sleep and sleep-wake manipulations in bipolar depression. Neuropsychobiology **45 Suppl 1**, 7–12, doi:10.1159/000049255 (2002).
42. Scott, J., Kallestad, H., Vedaa, O., Sivertsen, B. & Etain, B. Sleep disturbances and first onset of major mental disorders in adolescence and early adulthood: A systematic review and meta-analysis. Sleep Med Rev **57**, 101429, doi:10.1016/j.smrv.2021.101429 (2021).
43. Adamantidis, A. R., Gutierrez Herrera, C. & Gent, T. C. Oscillating circuitries in the sleeping brain. Nature Reviews Neuroscience **20**, 746–762, doi:10.1038/s41583-019-0223-4 (2019).
44. Purnell, B. S., Hajek, M. A. & Buchanan, G. F. Time-of-day influences on respiratory sequelae following maximal electroshock-induced seizures in mice. J Neurophysiol **118**, 2592–2600, doi:10.1152/jn.00039.2017 (2017).
45. Crochet, S. & Petersen, C. C. H. Correlating whisker behavior with membrane potential in barrel cortex of awake mice. Nature Neuroscience **9**, 608–610, doi:10.1038/nn1690 (2006).
46. Vyazovskiy, V. V. *et al.* Local sleep in awake rats. Nature **472**, 443–447, doi:10.1038/nature10009 (2011).
47. Sachdev, R. N. S. *et al.* Delta rhythm in wakefulness: evidence from intracranial recordings in human beings. Journal of Neurophysiology **114**, 1248–1254, doi:10.1152/jn.00249.2015 (2015).
48. Zhang, F. *et al.* Cross-Species Investigation on Resting State Electroencephalogram. Brain Topography **32**, 808–824, doi:10.1007/s10548-019-00723-x (2019).
49. Gereke, B. J., Mably, A. J. & Colgin, L. L. Experience-dependent trends in CA1 theta and slow gamma rhythms in freely behaving mice. J Neurophysiol **119**, 476–489, doi:10.1152/jn.00472.2017 (2018).
50. Vanderwolf, C. H. Hippocampal electrical activity and voluntary movement in the rat. Electroencephalography and Clinical Neurophysiology **26**, 407–418, doi:https://doi.org/10.1016/0013-4694(69)90092-3 (1969).
51. Zheng, C., Bieri, K. W., Trettel, S. G. & Colgin, L. L. The relationship between gamma frequency and running speed differs for slow and fast gamma rhythms in freely behaving rats. Hippocampus **25**, 924–938, doi:https://doi.org/10.1002/hipo.22415 (2015).
52. Goes, F. S. *et al.* Co-morbid anxiety disorders in bipolar disorder and major depression: familial aggregation and clinical characteristics of co-morbid panic disorder, social phobia, specific phobia and obsessive-compulsive disorder. Psychol Med **42**, 1449–1459, doi:10.1017/s0033291711002637 (2012).
53. Amerio, A., Odone, A., Liapis, C. C. & Ghaemi, S. N. Diagnostic validity of comorbid bipolar disorder and obsessive-compulsive disorder: a systematic review. Acta Psychiatr Scand **129**, 343–358, doi:10.1111/acps.12250 (2014).
54. De Stefano, L. A. *et al.* Developmental Effects on Auditory Neural Oscillatory Synchronization Abnormalities in Autism Spectrum Disorder. Front Integr Neurosci **13**, 34, doi:10.3389/fnint.2019.00034 (2019).

55. Bi, C. *et al.* Mutations of ANK3 identified by exome sequencing are associated with autism susceptibility. Hum Mutat **33**, 1635–1638, doi:10.1002/humu.22174 (2012).
56. Iqbal, Z. *et al.* Homozygous and heterozygous disruptions of ANK3: at the crossroads of neurodevelopmental and psychiatric disorders. Hum Mol Genet **22**, 1960–1970, doi:10.1093/hmg/ddt043 (2013).
57. Shi, L. *et al.* Whole-genome sequencing in an autism multiplex family. Mol Autism **4**, 8, doi:10.1186/2040-2392-4-8 (2013).
58. Zhu, S. *et al.* Genetic disruption of ankyrin-G in adult mouse forebrain causes cortical synapse alteration and behavior reminiscent of bipolar disorder. Proc Natl Acad Sci U S A **114**, 10479–10484, doi:10.1073/pnas.1700689114 (2017).
59. Gold, A. K. & Sylvia, L. G. The role of sleep in bipolar disorder. Nat Sci Sleep **8**, 207–214, doi:10.2147/nss.S85754 (2016).
60. Wang, Z. *et al.* Quantitative phosphoproteomic analysis of the molecular substrates of sleep need. Nature **558**, 435–439, doi:10.1038/s41586-018-0218-8 (2018).
61. Wagner, U., Gais, S. & Born, J. Emotional memory formation is enhanced across sleep intervals with high amounts of rapid eye movement sleep. Learn Mem **8**, 112–119, doi:10.1101/lm.36801 (2001).
62. Nishida, M., Pearsall, J., Buckner, R. L. & Walker, M. P. REM sleep, prefrontal theta, and the consolidation of human emotional memory. Cereb Cortex **19**, 1158–1166, doi:10.1093/cercor/bhn155 (2009).
63. van der Helm, E. & Walker, M. P. Sleep and Emotional Memory Processing. Sleep Med Clin **6**, 31–43, doi:10.1016/j.jsmc.2010.12.010 (2011).
64. Groch, S., Wilhelm, I., Diekelmann, S. & Born, J. The role of REM sleep in the processing of emotional memories: evidence from behavior and event-related potentials. Neurobiol Learn Mem **99**, 1–9, doi:10.1016/j.nlm.2012.10.006 (2013).
65. Montgomery, S. M. & Buzsáki, G. Gamma oscillations dynamically couple hippocampal CA3 and CA1 regions during memory task performance. Proc Natl Acad Sci U S A **104**, 14495–14500, doi:10.1073/pnas.0701826104 (2007).
66. Espinosa, F., Torres-Vega, M. A., Marks, G. A. & Joho, R. H. Ablation of Kv3. 1 and Kv3. 3 potassium channels disrupts thalamocortical oscillations in vitro and in vivo. Journal of Neuroscience **28**, 5570–5581 (2008).
67. Espinosa, F. *et al.* Alcohol hypersensitivity, increased locomotion, and spontaneous myoclonus in mice lacking the potassium channels Kv3. 1 and Kv3. 3. Journal of Neuroscience **21**, 6657–6665 (2001).
68. Joho, R. H., Ho, C. S. & Marks, G. A. Increased γ-and decreased δ-oscillations in a mouse deficient for a potassium channel expressed in fast-spiking interneurons. Journal of neurophysiology **82**, 1855–1864 (1999).
69. Joho, R. H., Street, C., Matsushita, S. & Knöpfel, T. Behavioral motor dysfunction in Kv3-type potassium channel-deficient mice. Genes, Brain and Behavior **5**, 472–482,

doi:https://doi.org/10.1111/j.1601-183X.2005.00184.x (2006).

70. Miyawaki, H., Watson, B. O. & Diba, K. Neuronal firing rates diverge during REM and homogenize during non-REM. Sci Rep **9**, 689, doi:10.1038/s41598-018-36710-8 (2019).
71. Lisman, John E. & Jensen, O. The Theta-Gamma Neural Code. Neuron **77**, 1002–1016, doi:https://doi.org/10.1016/j.neuron.2013.03.007 (2013).
72. Canolty, R. T. *et al.* High gamma power is phase-locked to theta oscillations in human neocortex. Science **313**, 1626–1628, doi:10.1126/science.1128115 (2006).
73. Sunaga, M. *et al.* The Characteristics of Power Spectral Density in Bipolar Disorder at the Resting State. Clin EEG Neurosci, 15500594211050487, doi:10.1177/15500594211050487 (2021).

Figures

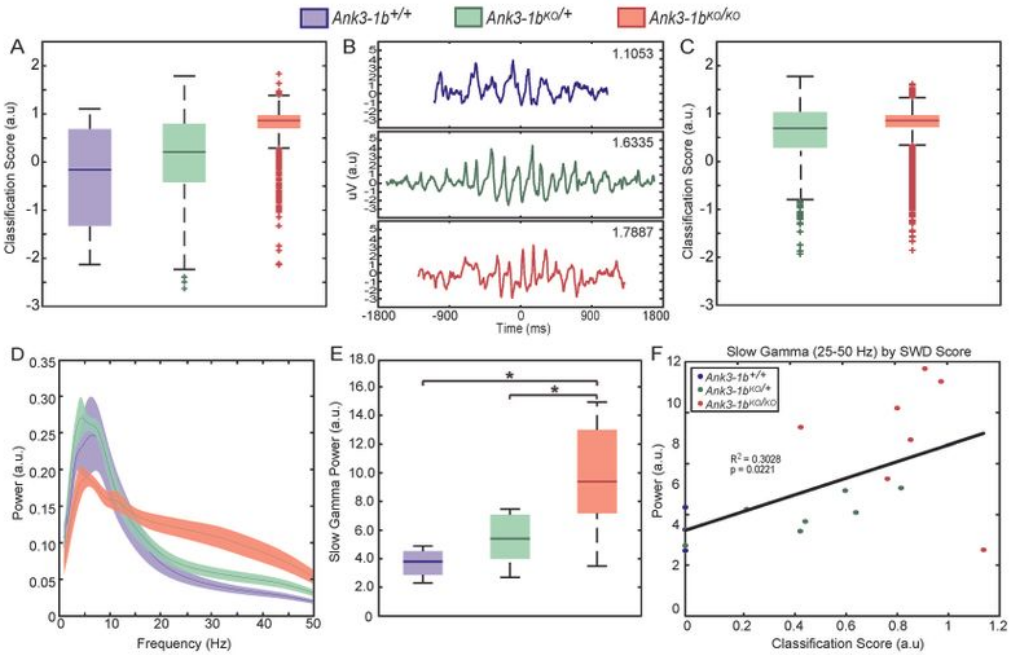

Figure 1—Seizure activity and slow gamma rhythms in *Ank3-1b* knockout mice. A: Boxplots of all positive and negative classification scores of SWD-like activity in EEG recordings from WT and *Ank3-1b*$^{KO/+}$ and *Ank3-1b*$^{KO/KO}$ mice. **B:** Example EEG trace from automated SWD prediction with highest classification score from each genotype. Note: the trace for the WT mouse does not meet requirements for classification as an SWD, demonstrating the need for manual validation. **C:** Boxplots of classification scores after manual verification of SWDs. Note: WT mice had no confirmed SWDs. **D:** Average power spectra for all recordings per genotype with 95% confidence intervals. **E:** Plots of estimated gamma power (25-45 Hz) for all recordings per genotype with 95% confidence intervals. Significant increases in gamma power are seen between *Ank3-1b*$^{KO/KO}$ and WT mice (*p = 0.024) and between *Ank3-1b*$^{KO/KO}$ and *Ank3-1b*$^{KO/+}$ (*p = 0.015). **F:** Positive correlation of gamma power and SWD classification score (R^2 = 0.30; *p = 0.02).

Figure 1

See image above for figure legend

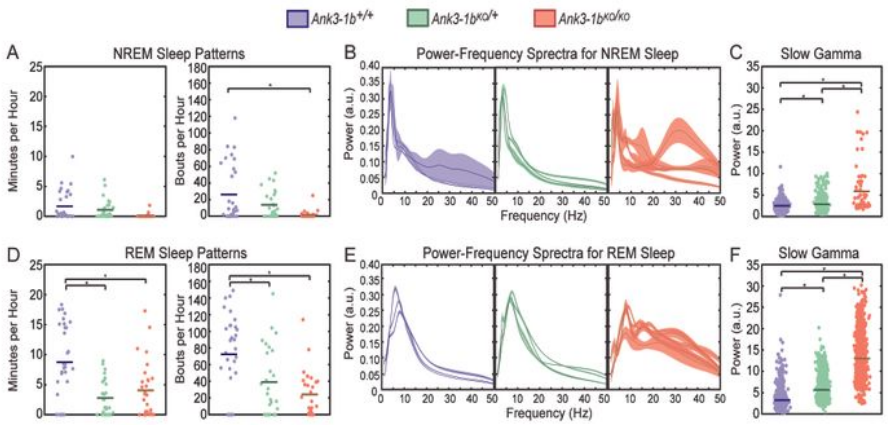

Figure 2—*Ank3-1b* knockout mice showed disturbed sleep patterns and increased slow gamma during sleep, with stronger effects observed during REM sleep than NREM. A: Plots of time spent in NREM (left) and frequency of NREM bouts (right) per hour in which each point represents an hour of measurement. *Ank3-1b*$^{KO/KO}$ mice have increased numbers of NREM bouts compared to WT mice (*p = 0.004). **B:** Individual plots of average power spectra during NREM sleep in which each plot represents power measured from an individual mouse with bootstrapped 95% confidence intervals showing variability in power between bouts. **C:** Plots of estimated gamma power (25-45 Hz) in which each point is a gamma power measurement during a NREM bout. *Ank3-1b* KO mice have increased slow gamma power compared to WT during NREM sleep (*Ank3-1b*$^{KO/KO}$ vs. WT: *p < 0.001; *Ank3-1b*$^{KO/+}$ vs. WT: *p = 0.001; *Ank3-1b*$^{KO/KO}$ vs. *Ank3-1b*$^{KO/+}$: *p < 0.001). **D:** Plots of time spent in REM (left) and frequency of REM bouts (right) per hour in which each point represents an hour of measurement. *Ank3-1b*$^{KO/+}$ and *Ank3-1b*$^{KO/KO}$ mice have decreased hourly REM sleep duration compared to WT (*p = 0.002 and *p = 0.03, respectively), and *Ank3-1b*$^{KO/KO}$ and *Ank3-1b*$^{KO/+}$ mice have decreased REM bouts per hour compared to WT (*p = 0.002 and *p < 0.001, respectively). **E:** Individual plots of average power spectra during REM sleep in which each plot represents an individual mouse with bootstrapped 95% confidence intervals showing variability in power between bouts. **F:** Plots of estimated gamma power (25-45 Hz) in which each point is a gamma power measurement during a REM bout. *Ank3-1b* KO mice have increased slow gamma compared to WT during REM sleep (*Ank3-1b*$^{KO/KO}$ vs. WT: *p < 0.001; *Ank3-1b*$^{KO/+}$ vs. WT: *p = 0.02; *Ank3-1b*$^{KO/KO}$ vs. *Ank3-1b*$^{KO/+}$: *p < 0.001).

Figure 2

See image above for figure legend

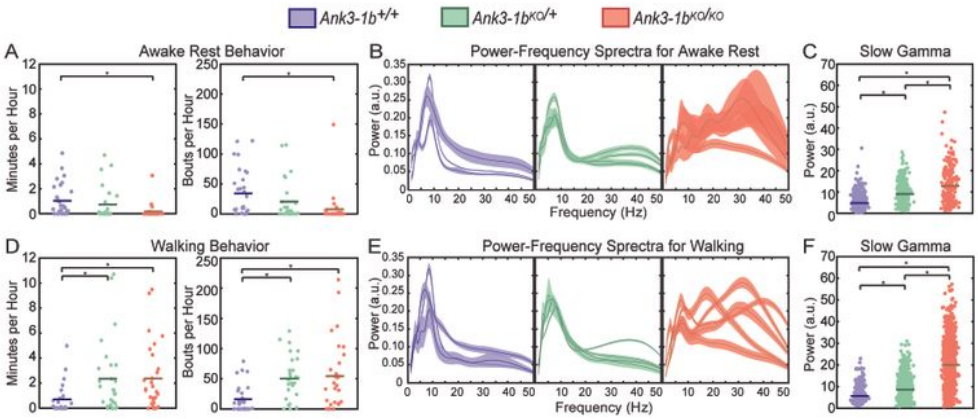

Figure 3—*Ank3-1b* knockout mice exhibited hyperactivity and increased slow gamma power during awake behaviors. A: Plots of time spent in awake rest per hour (left) and bouts of awake rest per hour (right) in which each point represents an hour of measurement. *Ank3-1b*$^{KO/KO}$ mice spent increased time in awake rest (*p = 0.006) and had increased bouts of awake rest (*p = 0.04) compared to WT mice. **B:** Individual plots of average power spectra during awake rest in which each plot represents an individual mouse with bootstrapped 95% confidence intervals showing variability in power between bouts. **C:** Plots of estimated gamma power (25-45 Hz) in which each point is a gamma power measurement during a bout of awake rest. *Ank3-1b* KO mice have increased slow gamma compared to WT mice during awake rest (*p < 0.001, for all comparisons). **D:** Plots of time spent walking per hour (left) and bouts of walking per hour (right) in which each point represents an hour of measurement. *Ank3-1b*$^{KO/KO}$ and *Ank3-1b*$^{KO/+}$ mice spent increased time (*p < 0.001 and *p = 0.04, respectively) and had increased bouts of walking per hour (*p = 0.002 and *p < 0.001, respectively) compared to WT mice. **E:** Individual plots of average power spectra during walking in which each plot represents an individual mouse with bootstrapped 95% confidence intervals showing variability in power between bouts. **F:** Plots of estimated gamma power (25-45 Hz) in which each point is a gamma power measurement during a bout of walking. *Ank3-1b* KO mice had increased slow gamma power compared to WT mice during walking (*p < 0.001, for all comparisons).

Figure 3

See image above for figure legend

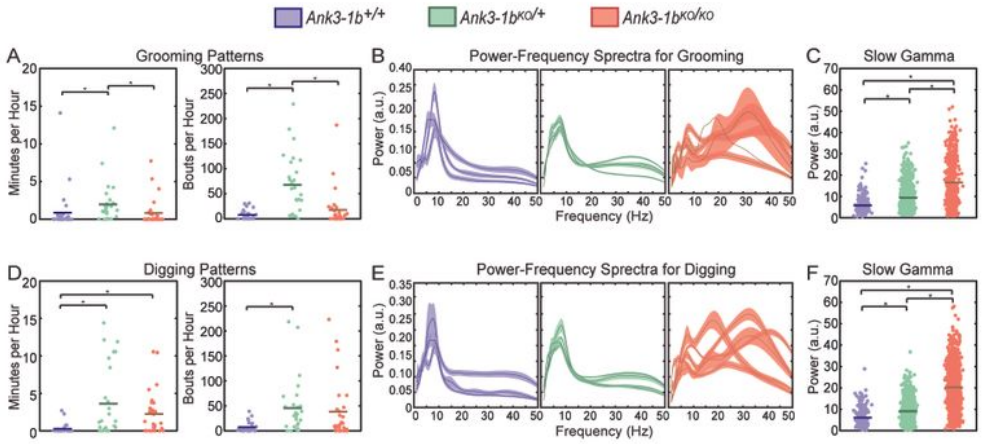

Figure 4—*Ank3-1b* knockout mice exhibited increased repetitive behaviors and increased slow gamma power during repetitive behaviors. A: Plots of grooming time (left) and grooming bouts (right) per hour in which each point represents an hour of measurement. *Ank3-1b*$^{KO/+}$ mice had increased repetitive grooming bouts compared to *Ank3-1b*$^{KO/KO}$ and WT mice (*p < 0.001, both), and spent more time grooming per hour compared to *Ank3-1b*$^{KO/KO}$ and WT mice (*p < 0.001, both). B: Individual plots of average power spectra during grooming in which each plot represents an individual mouse with bootstrapped 95% confidence intervals showing variability of power between bouts. C: Plots of estimated gamma power (25-45 Hz) in which each point is a gamma power measurement during a bout of grooming. *Ank3-1b* KO mice have increased slow gamma power compared to WT during grooming (*p < 0.001, for all comparisons). D: Plots of digging time (left) and digging bouts (right) per hour in which each point represents an hour of measurement. *Ank3-1b*$^{KO/+}$ and *Ank3-1b*$^{KO/KO}$ mice spent more time digging per hour compared to WT mice (*p = 0.02, both), and *Ank3-1b*$^{KO/+}$ mice had more digging bouts per hour compared to WT mice (*p = 0.002). E: Individual plots of average power spectra during digging in which each plot represents an individual mouse with bootstrapped 95% confidence intervals showing variability between bouts. F: Plots of estimated gamma power (25-45 Hz) in which each point is a gamma power measurement during a bout of digging. *Ank3-1b* KO mice had increased slow gamma power compared to WT mice during digging (*p < 0.001, for all comparisons).

Figure 4

See image above for figure legend

Supplementary Files

This is a list of supplementary files associated with this preprint. Click to download.

- supplementaryMaterialsFilesPage1.jpg
- supplementaryMaterialsFilesPage2.jpg
- supplementaryMaterialsFilesPage3.jpg
- SUPPLEMENTARYFIGURELEGENDS.docx
- SupplementaryFigure1.jpg
- SupplementaryFigure2.jpg
- SupplementaryFigure3.jpg